

# Measurement of the Dark Matter Velocity Dispersion with Galaxy Stellar Masses, UV Luminosities, and Reionization

Bruce Hoeneisen

Universidad San Francisco de Quito, Quito, Ecuador

Email: bhoeneisen@usfq.edu.ec

**How to cite this paper:** Hoeneisen, B. (2022) Measurement of the Dark Matter Velocity Dispersion with Galaxy Stellar Masses, UV Luminosities, and Reionization. *International Journal of Astronomy and Astrophysics*, 12, 258-272.

<https://doi.org/10.4236/ijaa.2022.123015>

**Received:** July 20, 2022

**Accepted:** September 18, 2022

**Published:** September 21, 2022

Copyright © 2022 by author(s) and Scientific Research Publishing Inc. This work is licensed under the Creative Commons Attribution International License (CC BY 4.0).

<http://creativecommons.org/licenses/by/4.0/>



Open Access

## Abstract

The root-mean-square of non-relativistic warm dark matter particle velocities scales as  $v_{\text{rms}}(a) = v_{\text{rms}}(1)/a$ , where  $a$  is the expansion parameter of the universe. This velocity dispersion results in a cut-off of the power spectrum of density fluctuations due to dark matter free-streaming. Let  $k_{\text{fs}}(t_{\text{eq}})$  be the free-streaming comoving cut-off wavenumber at the time of equal densities of radiation and matter. We obtain  $v_{\text{rms}}(1) = 0.41_{-0.12}^{+0.14}$  km/s, and  $k_{\text{fs}}(t_{\text{eq}}) = 2.0_{-0.5}^{+0.8}$  Mpc<sup>-1</sup>, at 68% confidence, from the observed distributions of galaxy stellar masses and rest frame ultra-violet luminosities. This result is consistent with reionization. From the velocity dispersion cut-off mass we obtain the limits  $v_{\text{rms}}(1) < 0.54$  km/s, and  $k_{\text{fs}}(t_{\text{eq}}) > 1.5$  Mpc<sup>-1</sup>. These results are in agreement with previous measurements based on spiral galaxy rotation curves, and on the formation of first galaxies and reionization. These measured parameters determine the temperature-to-mass ratio of warm dark matter. This ratio happens to be in agreement with the no freeze-in and no freeze-out warm dark matter scenario of spin 0 dark matter particles decoupling early on from the standard model sector. Spin 1/2 and spin 1 dark matter are disfavored if nature has chosen the no freeze-in and no freeze-out scenario. An extension of the standard model of quarks and leptons, with scalar dark matter that couples to the Higgs boson that is in agreement with all current measurements, is briefly reviewed. Discrepancies with limits on dark matter particle mass that can be found in the literature are addressed.

## Keywords

Warm Dark Matter, Galaxy Stellar Mass, Galaxy UV Luminosity, Reionization

## 1. Introduction

Let  $v_{hrms}(a)$  be the root-mean-square velocity of non-relativistic dark matter particles. This velocity dispersion scales with the expansion parameter  $a$  of the universe as  $v_{hrms}(a) = v_{hrms}(1)/a$  (assuming collisions, if any, do not excite internal degrees of freedom), so

$$v_{hrms}(1) = v_{hrms}(a)a = v_{hrms}(a) \left[ \frac{\Omega_c \rho_{crit}}{\rho_h(a)} \right]^{1/3}, \quad (1)$$

is an adiabatic invariant<sup>1</sup>.  $\rho_h(a)$  is the dark matter density. (We use the standard notation in cosmology, and parameters, as in [1]). In the cold dark matter  $\Lambda$ CDM cosmology it is assumed that dark matter velocity dispersion is negligible.  $v_{hrms}(1)$  is the single parameter that is added to the  $\Lambda$ CDM model to obtain the warm dark matter cosmology  $\Lambda$ WDM. Let  $P(k)$  be the power spectrum of relative density perturbations, referred to the present time, in the  $\Lambda$ CDM scenario.  $k$  is the comoving wavenumber. Then the power spectrum of  $\Lambda$ WDM is  $P(k)\tau^2(k)$ , where  $\tau^2(k)$  is a cut-off factor due to free-streaming of dark matter particles. At the time  $t_{eq}$  of equal radiation and matter densities, the free-streaming cut-off factor has the approximate form [2]

$$\tau^2(k) \approx \exp\left[-k^2/k_{fs}^2(t_{eq})\right], \quad (2)$$

where the comoving cut-off wavenumber is [2]

$$k_{fs}(t_{eq}) = \frac{1.455}{\sqrt{2}} \sqrt{\frac{4\pi G \bar{\rho}_m(1) a_{eq}}{v_{hrms}(1)^2}}, \quad (3)$$

where  $\bar{\rho}_m(1) \equiv \Omega_c \rho_{crit}$  is the dark matter density at the present time. At later times the Jeans mass decreases as  $a^{-3/2}$ , so non-linear regeneration of small scale structure becomes possible, and gives  $\tau^2(k)$  a ‘‘tail’’ when relative density perturbations approach unity. The challenge is to measure  $v_{hrms}(1)$  and  $k_{fs}(t_{eq})$ , and cross-check that their relation is consistent with (3).

$v_{hrms}(1)$  has been obtained from observed spiral galaxy rotation curves and Equation (1) [3] [4] [5].  $k_{fs}(t_{eq})$  has been obtained from observed galaxy stellar mass distributions [6], and from the redshift  $z$  of first galaxies and reionization [7]. In the present study we measure  $k_{fs}(t_{eq})$  with both galaxy stellar mass distributions and galaxy rest frame ultra-violet (UV) luminosity distributions. We also study reionization. These measurements are compared with the predictions of the no freeze-in and no freeze-out warm dark matter scenario as developed in [5]. Finally, an extension of the standard model of quarks and leptons that satisfies all current experimental constraints is briefly reviewed.

<sup>1</sup>Two ways to understand (1) are: 1) Consider an expanding universe. The velocity of a free particle with respect to that comoving observer that is momentarily at the position of the particle, is proportional to  $a^{-1}$ . To obtain this result use Hubble’s law with  $H = a^{-1} da/dt$ . 2) The adiabatic expansion of a collisional, or collisionless, noble gas satisfies  $T/\rho^{\gamma-1} = \text{constant}$ , with  $\gamma = 5/3$ . Since  $T \propto \langle v^2 \rangle$ , and  $\rho \propto a^{-3}$ ,  $\langle v^2 \rangle \propto a^{-2}$ .

## 2. Measurement of $k_{fs}(t_{eq})$

Observed distributions of galaxy stellar masses, and rest-frame UV luminosities, are compared with predictions for  $k_{fs}(t_{eq}) = 1, 2, 4$ , and  $1000 \text{ Mpc}^{-1}$  in **Figure 1** and **Figure 2**. The data on galaxy stellar masses  $M_*$  are obtained from the compilation in [8], with original measurements described in [9] [10] [11]. The data on the rest frame UV luminosities  $\nu L_{UV}$  are obtained from the compilation in [12] of measurements with the Hubble Space Telescope [13] [14], see also [15]. The UV luminosities have been corrected for dust extinction as described in [12] [16].  $\nu$  is the frequency corresponding to the wavelength  $1550 \text{ \AA}$ , and  $L_{UV}$  is the UV luminosity in units  $[\text{erg s}^{-1}\text{Hz}^{-1}]$ . In **Figure 1** are presented the observed distributions of stellar masses  $M_*$  and UV luminosities  $\nu L_{UV}$ , and the Press-Schechter [17] predicted distributions of the linear total (dark matter plus baryon) mass  $M$ , and its Sheth-Tormen ellipsoidal collapse extensions with parameter  $\nu \equiv 1.686/\sigma$  (not to be confused with the frequency above) and  $0.84\nu$  [18] [19]. Our default prediction uses  $0.84\nu$ . In **Figure 2** we add a

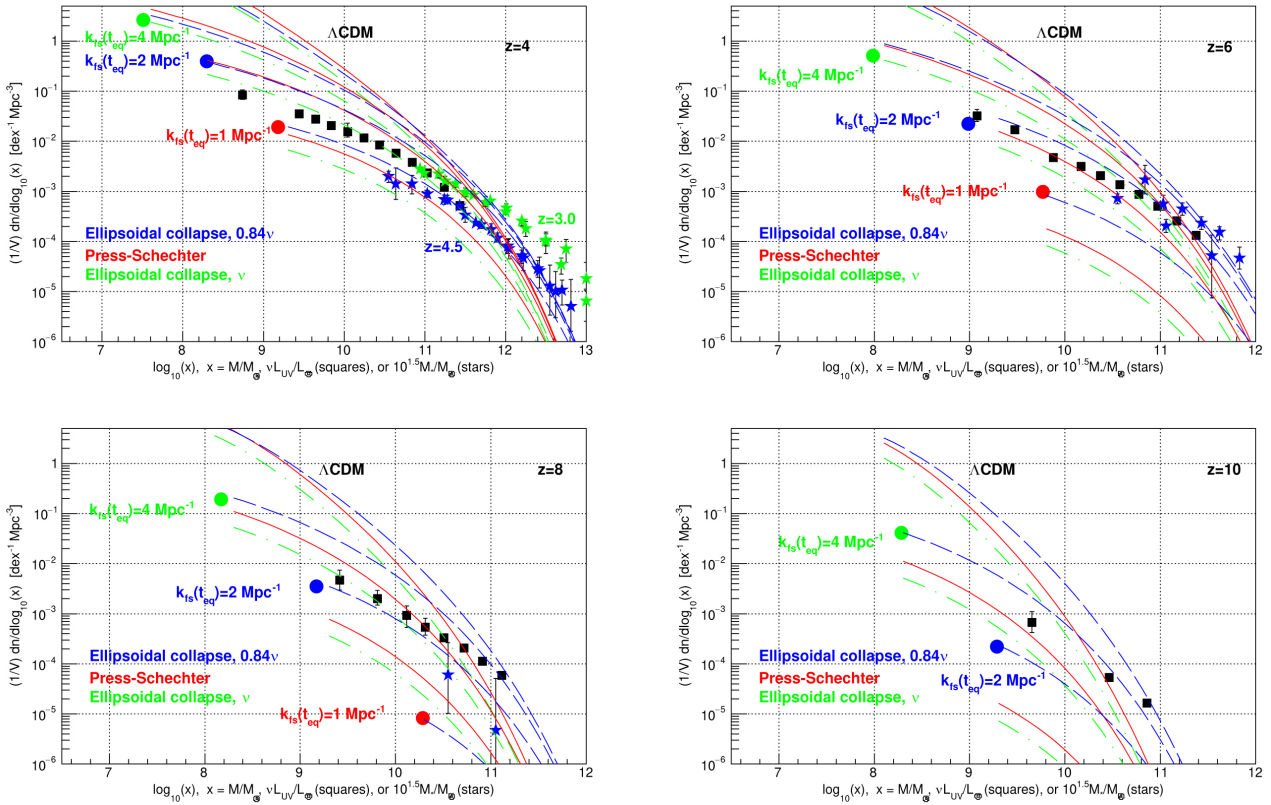


**Figure 1.** Shown are distributions of  $x$ , where  $x$  is the observed galaxy stellar mass  $M_*/M_\odot$  times  $10^{1.5}$  (stars), or the observed galaxy rest frame ultra-violet luminosity  $\nu L_{UV}/L_\odot$  (squares), or the predicted linear total (dark matter plus baryon) mass  $M/M_\odot$  (lines), at redshifts 4, 6, 8, and 10. The predictions correspond to  $k_{fs}(t_{eq}) = 1, 2, 4$  and  $1000 \text{ Mpc}^{-1}$ . The  $M_*/M_\odot$  data in the  $z=4$  panel correspond to  $z=3$  (green stars) and  $z=4.5$  (blue stars). The data sources and predictions are described in the main text. The round red, blue and green dots indicate the velocity dispersion cut-offs of the predictions [7] at  $k_{fs}(t_{eq}) = 1, 2$  and  $4 \text{ Mpc}^{-1}$ , respectively.

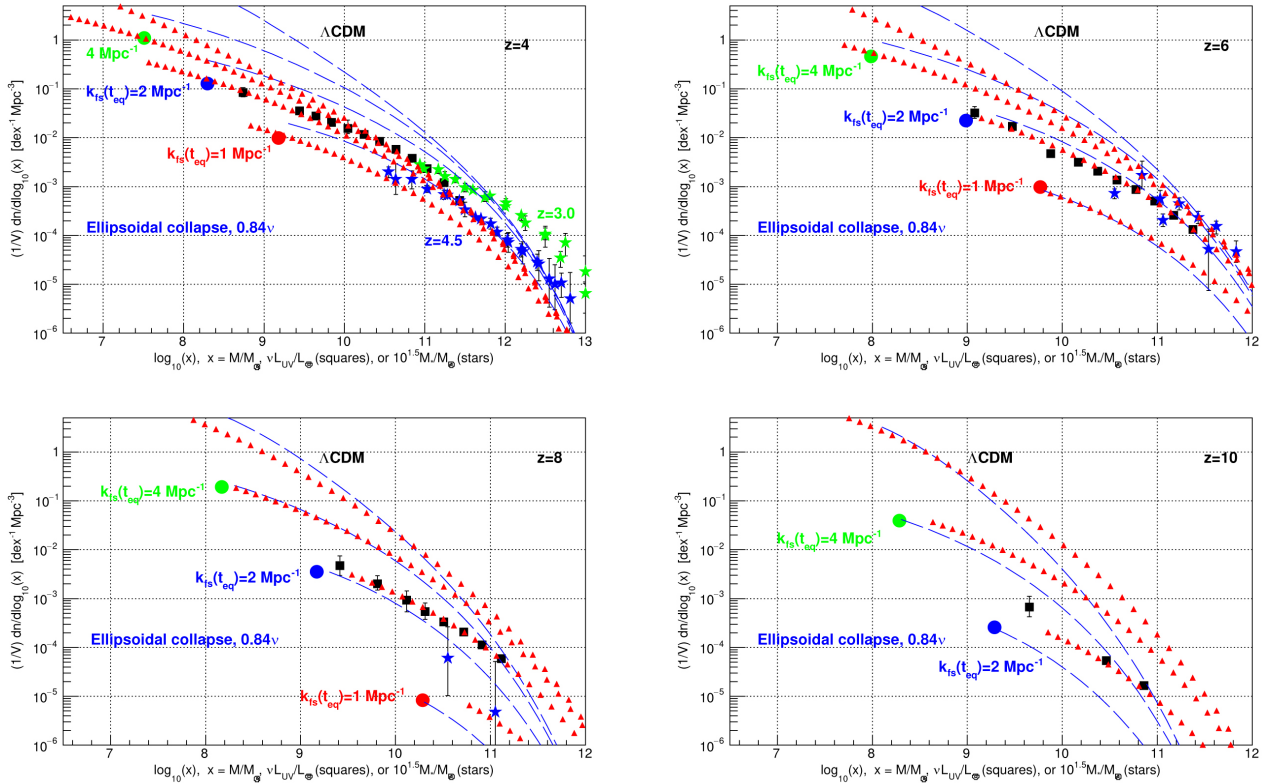


**Figure 2.** Shown are distributions of  $x$ , where  $x$  is the observed galaxy stellar mass  $M_*/M_\odot$  times  $10^{1.5}$  (stars), or the observed galaxy rest frame ultra-violet luminosity  $\nu L_{UV}/L_\odot$  (squares), or the predicted linear total (dark matter plus baryon) mass  $M/M_\odot$  (dashed line), or the predicted  $\nu L_{UV}/L_\odot$  (triangles) at redshifts 4, 6, 8, and 10. The predictions correspond to  $k_{is}(t_{eq})=1, 2, 4$  and  $1000 \text{ Mpc}^{-1}$ . The  $M_*/M_\odot$  data in the  $z=4$  panel correspond to  $z=3$  (green stars) and  $z=4.5$  (blue stars). The data sources and predictions are described in the main text. The round red, blue and green dots indicate the velocity dispersion cut-offs of the predictions [7] at  $k_{is}(t_{eq})=1, 2$  and  $4 \text{ Mpc}^{-1}$ , respectively.

comparison with the predicted UV luminosity distributions. The adimensional observables in the figures are  $10^{1.5} M_*/M_\odot$ ,  $\nu L_{UV}/L_\odot$ , and  $M/M_\odot$ , where  $M_\odot = 1.988 \times 10^{30} \text{ kg}$  is the solar mass, and  $L_\odot = 3.8 \times 10^{33} \text{ erg} \cdot \text{s}^{-1}$  is the bolometric solar luminosity. The measured UV AB-magnitudes are converted to luminosity as follows:  $M_{UV} \approx 5.9 - 2.5 \log_{10}(\nu L_{UV}/L_\odot)$  [12].

The Press-Schechter prediction depends on the variance of the relative density perturbation  $\delta(\mathbf{x}) \equiv (\rho(\mathbf{x}) - \bar{\rho})/\bar{\rho}$  on the linear total (dark matter plus baryon) mass scale  $M$ , at redshift  $z$  [20]

$$\sigma^2(M, z, k_{is}) = \frac{f^2}{(2\pi)^3 (1+z)^2} \int_0^\infty 4\pi k^2 dk P(k) \tau^2(k) W^2(k), \quad (4)$$

and so depends on the assumed free-streaming cut-off factor  $\tau^2(k)$ , and on the window function  $W(k)$  that defines the linear mass scale  $M$ . We consider two window functions: the Gaussian window function

$$W(k) = \exp\left(-\frac{k^2}{2k_0^2}\right), \quad M = \frac{4}{3} \pi \left(\frac{1.555}{k_0}\right)^3 \bar{\rho}_m, \quad (5)$$

and, in Section 3, the sharp- $k$  window function  $W(k)=1$  for  $k \leq k_0$ ,  $W(k)=0$  for  $k > k_0$ , and

$$M_h = \frac{4}{3} \pi \left( \frac{c}{k_0} \right)^3 \bar{\rho}_h. \tag{6}$$

**Figure 1** and **Figure 2** are obtained with the free-streaming cut-off function with a non-linear regenerated “tail” [5]

$$\tau^2(k) = \begin{cases} \exp\left(-\frac{k^2}{k_{fs}^2(t_{eq})}\right) & \text{if } k < k_{fs}(t_{eq}), \\ \exp\left(-\frac{k^n}{k_{fs}^n(t_{eq})}\right) & \text{if } k \geq k_{fs}(t_{eq}), \end{cases} \tag{7}$$

with  $n=1$ , and the Gaussian window function. The parameter  $n$  allows a study of the effect of the non-linear regenerated tail on the measurement. As we shall see later on in Section 3, the results are insensitive to  $n$  in the range 0.2 to 1.1, and in this range of  $n$ , the Gaussian and sharp- $k$  window functions obtain approximately the same results. The  $\Lambda$ WDM power spectrum  $P(k)\tau^2(k)$  is normalized, for each  $k_{fs}(t_{eq})$ , so that  $\sigma_8 = 0.811$  with a top-hat window function of radius  $r = 8/h \text{ Mpc} = 8/0.674 \text{ Mpc}$  [1].

Let us comment on masses. The linear perturbation mass scale  $M$  in the Press-Schechter formalism is well defined, since the linear perturbation dimensions scale as  $a$ , and the density scales as  $a^{-3}$ , so  $M$  is independent of the expansion parameter  $a$ . However, in the warm dark matter scenario, the dark matter halo mass is ill defined: the halo radius grows with a constant velocity, and the halo mass grows linearly with time indefinitely [21]. The relation between the linear perturbation mass  $M$  and the final galaxy stellar mass  $M_*$  is non-trivial: not only must the galaxy halo form, but the baryons must lose energy by radiation until the baryon density  $\rho_b(r)$  decreases faster than  $r^{-3}$  at large radius  $r$ , so  $M_*$  becomes finite and well defined [7]. However, the comparison between predictions and observations in **Figure 1** and **Figure 2** offers a useful empirical relation between the observables:

$$\frac{\nu L_{UV}}{L_\odot} \equiv a \frac{M_*}{M_\odot} \equiv b \frac{M}{M_\odot}, \tag{8}$$

where  $a \approx 10^{1.5}$  (as in [6]), and  $b \approx 1$ , independently of  $M$  or  $z$ . (A more detailed analysis could take  $a$  and  $b$  to be functions of  $M$  and  $z$ , e.g.  $a \approx 10^2$  at  $z=8$ , see **Figure 1**). The factor  $1/a \approx 10^{-1.5}$  is equal to  $0.2\Omega_b/(\Omega_c + \Omega_b)$ , indicating that approximately 20% of the original baryons in the linear density perturbation that forms the galaxy, ends up in the galaxy stars.

How is the UV luminosity predicted? The Press-Schechter relation or its Sheth-Tormen ellipsoidal collapse extensions, obtain the numbers of collapsed halos in bins of  $\log_{10} M$  and  $z$ . From (8) we obtain  $\log_{10} M_*$ . This allows the calculation of the star formation rate (SFR). Finally, the rest frame UV luminosity per galaxy is obtained from

$$\frac{\nu L_{UV}}{L_{\odot}} = 10^{9.61} \times \left( \frac{\text{SFR per halo}}{M_{\odot} \cdot \text{yr}^{-1}} \right), \quad (9)$$

as in [22]. In **Figure 2** note the excellent agreement of  $\nu L_{UV}/L_{\odot}$  data and predictions for all  $z$  and  $M$ .

Now a word on the *velocity dispersion* cut-off. If dark matter is warm, the formation of galaxies has two cut-offs: the *free-streaming* cut-off due to the free-streaming cut-off factor  $\tau^2(k)$  in the power spectrum of density perturbations, and the *velocity dispersion* cut-off [7]. In the  $\Lambda$ CDM cosmology, when a spherically symmetric relative density perturbation  $(\rho - \bar{\rho})/\bar{\rho}$  reaches 1.686 in the linear approximation, the exact solution diverges and a galaxy forms. The same is true in the  $\Lambda$ WDM scenario if the linear total perturbation mass  $M$  exceeds the *velocity dispersion* cut-off  $M_{vd}$ . The *velocity dispersion* cut-off  $M_{vd}$  is obtained by numerical integration of hydro-dynamical equations [7], with results summarized in **Table 1**, and indicated, in **Figures 1-4**, by red, blue, and green dots for  $k_{fs}(t_{eq}) = 1, 2$ , and  $4 \text{ Mpc}^{-1}$ , respectively. Below the *velocity*

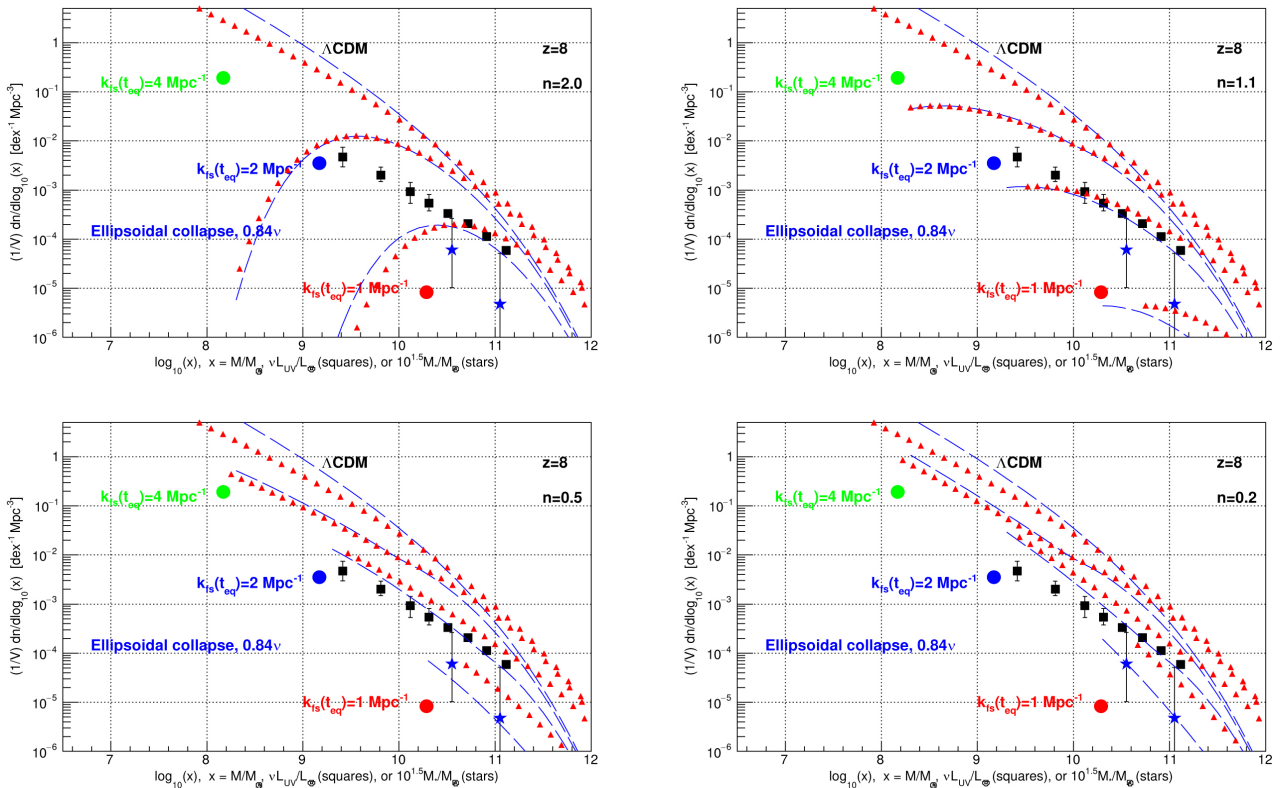


**Figure 3.** Shown are distributions of  $x$ , where  $x$  is the observed galaxy stellar mass  $M_*/M_{\odot}$  times  $10^{1.5}$  (stars), or the observed galaxy rest frame ultra-violet luminosity  $\nu L_{UV}/L_{\odot}$  (squares), or the predicted linear total (dark matter plus baryon) mass  $M/M_{\odot}$  (dashed line), or the predicted  $\nu L_{UV}/L_{\odot}$  (triangles), at redshift 8. The predictions correspond to  $k_{fs}(t_{eq}) = 1, 2, 4$  and  $1000 \text{ Mpc}^{-1}$ . The free-streaming cut-off factor is  $\tau^2(k)$ , with a “tail” as in (3), with  $n = 2.0, 1.1, 0.5$ , or  $0.2$ . The window function is sharp- $k$ .  $n = 2$  corresponds to no non-linear regenerated tail. The round red, blue and green dots indicate the velocity dispersion cut-offs of the predictions [7] at  $k_{fs}(t_{eq}) = 1, 2$  and  $4 \text{ Mpc}^{-1}$ , respectively. Note that  $k_{fs} = 1 \text{ Mpc}^{-1}$  is ruled out by the velocity dispersion cut-off, indicated by a red dot.

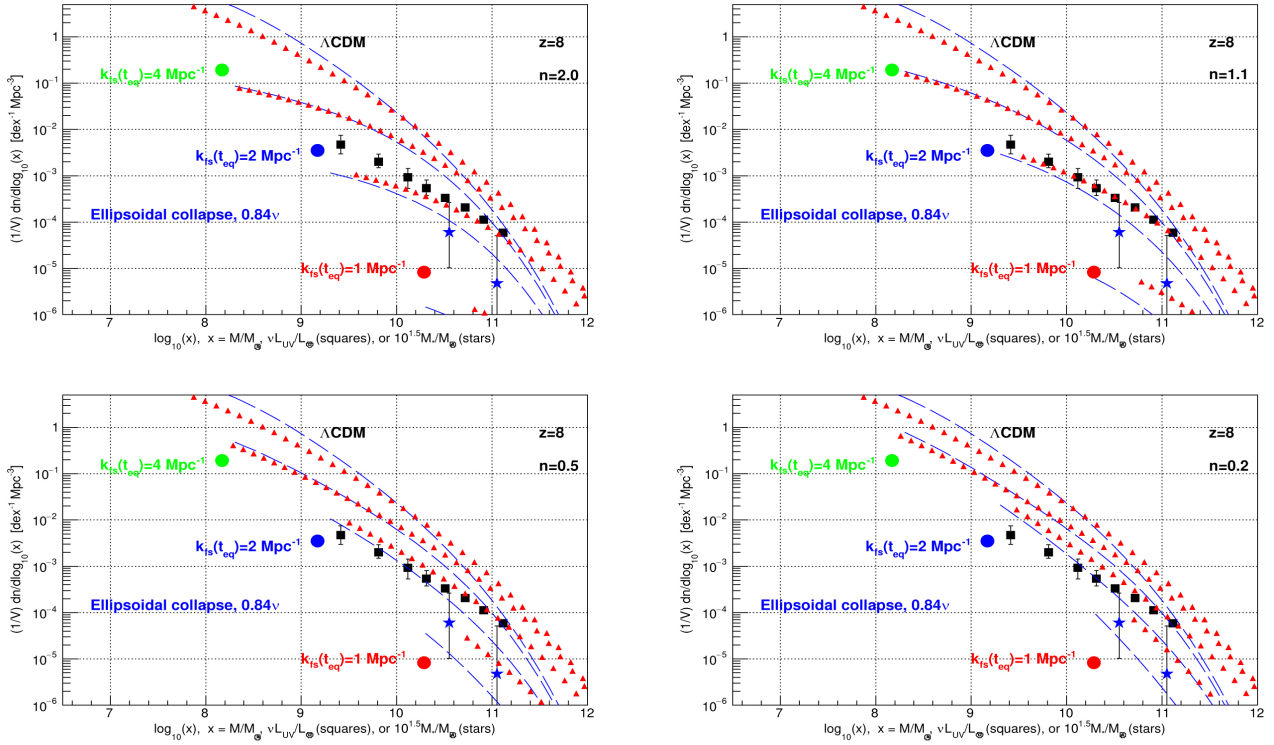


Figure 4. Same as Figure 3 except that the window function is Gaussian instead of sharp- $k$ .

Table 1. Shown is the velocity dispersion cut-off mass  $M_{vd}$  of the linear total (dark matter plus baryon) mass  $M$ , as a function of redshift  $z$ , and free-streaming comoving cut-off wavenumber  $k_{fs}(t_{eq})$ . At this cut-off mass  $M_{vd}$ , velocity dispersion delays galaxy formation by  $\Delta z=1$  (obtained from numerical integration of hydro-dynamical equations [7]).

| $z$ | $k_{fs}(t_{eq})$ | $M_{vd}$          | $z$ | $k_{fs}(t_{eq})$ | $M_{vd}$           |
|-----|------------------|-------------------|-----|------------------|--------------------|
|     | [Mpc $^{-1}$ ]   | [ $M_{\odot}$ ]   |     | [Mpc $^{-1}$ ]   | [ $M_{\odot}$ ]    |
| 4   | 1                | $1.5 \times 10^9$ | 8   | 1                | $2 \times 10^{10}$ |
| 4   | 1.66             | $3 \times 10^8$   | 8   | 1.66             | $4 \times 10^9$    |
| 4   | 2                | $2 \times 10^8$   | 8   | 2                | $1.5 \times 10^9$  |
| 4   | 4                | $3 \times 10^7$   | 8   | 4                | $1.5 \times 10^8$  |
| 6   | 1                | $6 \times 10^9$   | 10  | 1                | $2 \times 10^{10}$ |
| 6   | 1.66             | $2 \times 10^9$   | 10  | 1.66             | $4.5 \times 10^9$  |
| 6   | 2                | $1 \times 10^9$   | 10  | 2                | $2 \times 10^9$    |
| 6   | 4                | $1 \times 10^8$   | 10  | 4                | $2 \times 10^8$    |

dispersion cut-off mass  $M_{vd}$ , the galaxy formation is delayed, and finally no self-gravitating structure forms. The Press-Schechter formalism includes the free-streaming cut-off, but not the velocity dispersion cut-off. Care must be taken not to apply the Press-Schechter formalism below the velocity dispersion

cut-off, and care must be taken to include the non-linear regenerated tail of  $\tau^2(k)$ .

The comparison of data and predictions in **Figure 1** favor  $k_{\text{fs}}(t_{\text{eq}}) \approx 1.5 \text{ Mpc}^{-1}$  at  $z = 4$ , increasing to  $k_{\text{fs}}(t_{\text{eq}}) \approx 3.0 \text{ Mpc}^{-1}$  at  $z = 10$ . The comparison of data and predictions in **Figure 2** is consistent with  $k_{\text{fs}}(t_{\text{eq}}) \approx 2 \text{ Mpc}^{-1}$  for  $z = 4, 6, 8$  and 10. From **Figure 1** and **Figure 2**, and studies to be presented in Section 3, we obtain

$$v_{\text{hrms}}(1) = 0.41_{-0.12}^{+0.14} \text{ km/s} \quad \text{and} \quad k_{\text{fs}}(t_{\text{eq}}) = 2.0_{-0.5}^{+0.8} \text{ Mpc}^{-1}, \quad (10)$$

at 68% confidence.

### 3. Non-Linear Regeneration of Small Scale Structure

After equality of the densities of radiation and matter, the Jeans mass decreases as  $a^{-3/2}$ , allowing regeneration of small scale structure as soon as relative density perturbations approach unity. The importance of this regeneration is studied with warm dark matter only simulations in [23], indicating that small scale structure regeneration should not be neglected. The uncertainty of the small scale structure regeneration contributes to the uncertainty of the measured  $k_{\text{fs}}(t_{\text{eq}})$ . To estimate this uncertainty, we perform a data driven study by repeating **Figure 2** with  $\tau^2(k)$  with a regenerated tail as in (7), with  $n = 2.0, 1.1, 0.5$  and 0.2, and with the sharp- $k$  window function. (Note: The sharp- $k$  window function is ill defined in  $r$ -space [5], and has no well-defined mass  $M$ , so the parameter  $c$  in (6) is fixed from simulations to  $c \approx 2.7$ . However, the value of  $c$  does not change the measurement of  $k_{\text{fs}}(t_{\text{eq}})$ , as its effect can be absorbed into the parameter  $b$ . To avoid changing the value of  $b = 1$ , we set  $c = 1.555$  [5]). The results, for  $z = 8$ , are presented in **Figure 3**. Agreement of observations with data is good in a wide range of  $n$ , *i.e.*  $0.5 \lesssim n \lesssim 1.1$ , with  $1.6 \text{ Mpc}^{-1} \lesssim k_{\text{fs}}(t_{\text{eq}}) \lesssim 2.0 \text{ Mpc}^{-1}$ . For comparison, **Figure 4** is the same as **Figure 3**, except that the Gaussian window function replaces the sharp- $k$  window function. The results with these two window functions are approximately the same, except when the non-linear regenerated tail is absent, *i.e.* when  $n \rightarrow 2$ .

The lessons learned from the studies in this section are as follows. Nature, and simulations [5] [23], do indeed add a non-linear regenerated tail to the free-streaming cut-off factor  $\tau^2(k)$ . With this tail, approximately the same predicted distributions are obtained with the sharp- $k$  or Gaussian window functions, and the predictions are in agreement with the data, so long as  $0.5 \lesssim n \lesssim 1.1$ . The Gaussian window function is well behaved in both  $r$ -space and  $k$ -space. The sharp- $k$  window function is ill behaved in  $r$ -space, and does not obtain a well defined mass  $M$ . Using the cut-off factor  $\tau^2(k)$  without a non-linear regenerated tail, together with the sharp- $k$  window function, leads to several published limits, of order keV, on the warm dark matter “thermal relic mass” that do not correspond to nature (which does indeed regenerate a tail to  $\tau^2(k)$ , that should not be neglected).

### 4. Reionization

The universe is neutral from redshift  $z \approx 1000$  to  $z \approx 10$  when first stars start reionizing hydrogen and helium. The bulk of reionization occurs in the interval from  $z = 8$  to  $z = 6$ . Thereafter hydrogen is highly ionized. For  $z \lesssim 4$ , helium becomes doubly ionized. The free-electrons scatter the cosmic microwave background radiation resulting in a reionization optical depth  $\tau = 0.054 \pm 0.007$  measured by the Planck collaboration [1] (corresponding to an instantaneous reionization at  $z = 7.4$ ). The measured  $\tau$  implies that the luminosity distributions have a cut-off [12] [24], else the calculated  $\tau$  is greater than observed. This is the *velocity dispersion* cut-off as presented in **Table 1** (not the *free-streaming* cut off with a non-linear regenerated “tail”, and probably not a baryon physics cut-off). From **Table 2** we obtain agreement between the Planck measurement and the velocity dispersion cut-off, and estimate.

$$v_{\text{rms}}(1) \approx 1.2 \text{ to } 0.15 \text{ km/s and } k_{\text{fs}}(t_{\text{eq}}) \approx 0.7 \text{ to } 5.4 \text{ Mpc}^{-1}. \quad (11)$$

Note that **Table 2** confirms that the *velocity dispersion* cut-off has physical consequences, and implies that dark matter is indeed warm, not cold.

### 5. The Velocity Dispersion Cut-Off Limit

Let us assume that the faintest UV luminosity data points in the figures are due to the velocity dispersion cut-offs. This assumption obtains an upper bound to  $v_{\text{rms}}(1)$ , and a lower bound to  $k_{\text{fs}}(t_{\text{eq}})$ . Allowing a factor 3 uncertainty on the velocity dispersion cut-off masses  $M_{\text{vd}}$  in **Table 1** (e.g. at what  $\Delta z$  should  $M_{\text{vd}}$  be defined?), we obtain

$$v_{\text{rms}}(1) < 0.54 \text{ km/s and } k_{\text{fs}}(t_{\text{eq}}) > 1.5 \text{ Mpc}^{-1}, \quad (12)$$

at 95% confidence. Note that the faintest UV luminosity data points in the figures already saturate the reionization optical depth measured by the Planck collaboration, see **Table 2**, and so should be near the velocity dispersion cut-offs. A dedicated search for the cut-off of  $M_{\text{UV}}$  as a function of  $z$  is in order.

**Table 2.** At  $z = 8$ , for each  $k_{\text{fs}}(t_{\text{eq}})$  are presented the velocity dispersion cut-off  $M_{\text{vd}}/M_{\odot}$  of the linear total (dark matter plus baryon) mass  $M/M_{\odot} \approx \nu L_{\text{UV}}/L_{\odot}$  from **Table 1**, the corresponding cut-off AB-magnitude  $M_{\text{UV}} \approx 5.9 - 2.5 \log_{10}(\nu L_{\text{UV}}/L_{\odot})$ , and the corresponding reionization optical depth  $\tau$  from Figure 13 of [24]. A somewhat lower value of  $\tau$  is obtained from Figure 2 of [12]. The Planck collaboration obtains  $\tau = 0.054 \pm 0.007$  [1].

| $k_{\text{fs}}(t_{\text{eq}})$ | $M_{\text{vd}}/M_{\odot}$ | $M_{\text{UV}}$ cut-off | $\tau$            |
|--------------------------------|---------------------------|-------------------------|-------------------|
| 1 $\text{Mpc}^{-1}$            | $2 \times 10^{10}$        | -19.9                   | $0.047 \pm 0.006$ |
| 2 $\text{Mpc}^{-1}$            | $1.5 \times 10^9$         | -17.0                   | $0.053 \pm 0.006$ |
| 4 $\text{Mpc}^{-1}$            | $1.5 \times 10^8$         | -14.5                   | $0.060 \pm 0.008$ |

## 6. The No Freeze-In and No Freeze-Out Warm Dark Matter Scenario

**Table 3** summarizes measurements of the velocity dispersion  $v_{\text{rms}}(1)$ , and the free-streaming comoving cut-off wavenumber  $k_{\text{fs}}(t_{\text{eq}})$ , as well as the no freeze-in and no freeze-out warm dark matter scenario predictions (as developed in [5]). **Table 3** updates **Table 1** of [5]. Measurements of  $v_{\text{rms}}(1)$  are obtained from rotation curves of 56 spiral galaxies [3] [4] [5]. Measurements of  $k_{\text{fs}}(t_{\text{eq}})$  are obtained from galaxy stellar mass distributions at  $z = 4.5, 6, 7$  and 8 [6]. These measurements are indeed related by the free-streaming Equation (3), within the measurement uncertainties, confirming that  $k_{\text{fs}}(t_{\text{eq}})$  is due to free-streaming. Measurements of  $v_{\text{rms}}(1)$  and  $k_{\text{fs}}(t_{\text{eq}})$  are also obtained from the formation of first galaxies and reionization [7], and from the present measurements (10), (11) and (12). These measurements determine the temperature-to-mass ratio  $T_h(a)/m_h$  of dark matter. This ratio happens to be in agreement with the no freeze-in and no freeze-out warm dark matter scenario for spin 0 dark matter particles that decouple early on from the standard model sector, see **Table 3**.

We note that  $k_{\text{fs}}(t_{\text{eq}}) \approx 1 \text{ Mpc}^{-1}$  is disfavored for several reasons:

- From the comparison of data and predictions in **Figure 1** and **Figure 2**.
- First galaxies and reionization are delayed with respect to observations [7].

**Table 3.** Summary of measurements of the warm dark matter velocity dispersion  $v_{\text{rms}}(1)$ , and the free-streaming comoving cut-off wavenumber  $k_{\text{fs}}(t_{\text{eq}})$ , as well as the predictions of the no freeze-in and no freeze-out warm dark matter scenario [5].  $a'_{\text{hNR}} \equiv v_{\text{rms}}(1)/c$  is the expansion parameter at which dark matter becomes non-relativistic. After  $e^+e^-$  annihilation, while dark matter is ultra-relativistic,  $0.424 \geq T_h/T \geq 0.344$ , corresponding to dark matter decoupling from the standard model sector at  $T_C < T_{\text{dec}} < m_\tau$ . \* For spin 1 dark matter the predictions are model dependent [25]. \*\* Majorana neutrino.

| Observable                     | $v_{\text{rms}}(1)$ [km/s] | $10^6 a'_{\text{hNR}}$ | $k_{\text{fs}}(t_{\text{eq}})$ [Mpc $^{-1}$ ] | $m_h$ [eV]       |
|--------------------------------|----------------------------|------------------------|---|------------------|
| Spiral galaxies [3] [4] [5]    | $0.79 \pm 0.33$            | $2.64 \pm 1.10$        | $1.03^{+0.74}_{-0.30}$                        |                  |
| $M_*$ distribution [6]         | $0.91^{+0.72}_{-0.30}$     | $3.02^{+2.42}_{-0.99}$ | $0.90^{+0.44}_{-0.40}$                        |                  |
| First galaxies [7]             | $\approx 0.4$ to $0.2$     | $\approx 1.4$ to $0.7$ | $\approx 2$ to $4$                            |                  |
| $M_*$ and $L_{\text{UV}}$ (10) | $0.41^{+0.14}_{-0.12}$     | $1.36^{+0.45}_{-0.39}$ | $2.0^{+0.8}_{-0.5}$                           |                  |
| Reionization (11)              | $\approx 1.2$ to $0.15$    | $\approx 3.9$ to $0.5$ | $\approx 0.7$ to $5.4$                        |                  |
| Vel. disp. cut-off (12)        | $< 0.54$                   | $< 1.8$                | $> 1.5$                                       |                  |
| Fermions spin 1/2**            |                            |                        |   |                  |
| No freeze-in/-out              | 1.93 to <b>0.83</b>        | 6.43 to <b>2.78</b>    | 0.42 to <b>0.98</b>                           | 54 to <b>101</b> |
| Bosons                         |                            |                        |   |                  |
| No fr-in/-out spin 0           | 1.12 to <b>0.48</b>        | 3.73 to <b>1.61</b>    | 0.73 to <b>1.69</b>                           | 81 to <b>152</b> |
| No fr-in/-out spin 1*          | 2.24 to <b>0.97</b>        | 7.46 to <b>3.22</b>    | 0.36 to <b>0.84</b>                           | 40 to <b>76</b>  |

- The velocity dispersion cut-off obtains the limits in (12). For example, at  $z = 8$  and  $k_{fs}(t_{eq}) = 1 \text{ Mpc}^{-1}$ ,  $M_{vd}/M_{\odot} = 2 \times 10^{10} \approx \nu L_{UV}/L_{\odot}$ , see **Table 1**, while the distribution of  $\nu L_{UV}/L_{\odot}$  extends below this cut-off to  $2.5 \times 10^9$ , see **Figure 2**.

In conclusion, if nature has chosen the no freeze-in and no freeze-out scenario of [5], the spin 1/2 and spin 1 dark matter alternatives are disfavored. We note that the measurements favor scalar, *i.e.* spin 0, dark matter that decouples early on from the standard model sector, e.g. scalar dark matter coupled to the Higgs boson. In this case, the dark matter particle mass is  $m_h = 150 \pm 2 \text{ eV}$ , with the uncertainty mainly determined by the uncertainty of  $\Omega_c h^2$  [5]. Also, in this case,

$$v_{rms}(1) = 0.49 \pm 0.01 \text{ km/s} \text{ and } k_{fs}(t_{eq}) = 1.66 \pm 0.03 \text{ Mpc}^{-1}. \quad (13)$$

### 7. Adding Dark Matter to the Standard Model

The (arguably) simplest renormalizable extensions of the standard model to add spin 0, 1/2, or 1 warm dark matter, that are in agreement with the no freeze-in and no freeze-out scenario, are presented in [25]. Here we revise the spin 0 case with  $m_h = 150 \pm 2 \text{ eV}$  for the particular scenario developed in [5]. The Lagrangian is

$$\mathcal{L} = \mathcal{L}_{SM} + \frac{1}{2} \partial_{\mu} S \cdot \partial^{\mu} S - \frac{1}{2} \bar{m}_S^2 S^2 - \frac{\lambda_S}{4!} S^4 - \dots - \frac{1}{2} \lambda_{hS} (\phi^{\dagger} \phi) S^2, \quad (14)$$

where  $\mathcal{L}_{SM}$  is the standard model Lagrangian,  $S$  is a real scalar Klein Gordon dark matter field with  $Z_2$  symmetry  $S \leftrightarrow -S$ , and  $\phi$  is the Higgs boson field. The no freeze-in condition, that dark matter attains thermal and diffusive equilibrium with the standard model sector before the temperature of the universe

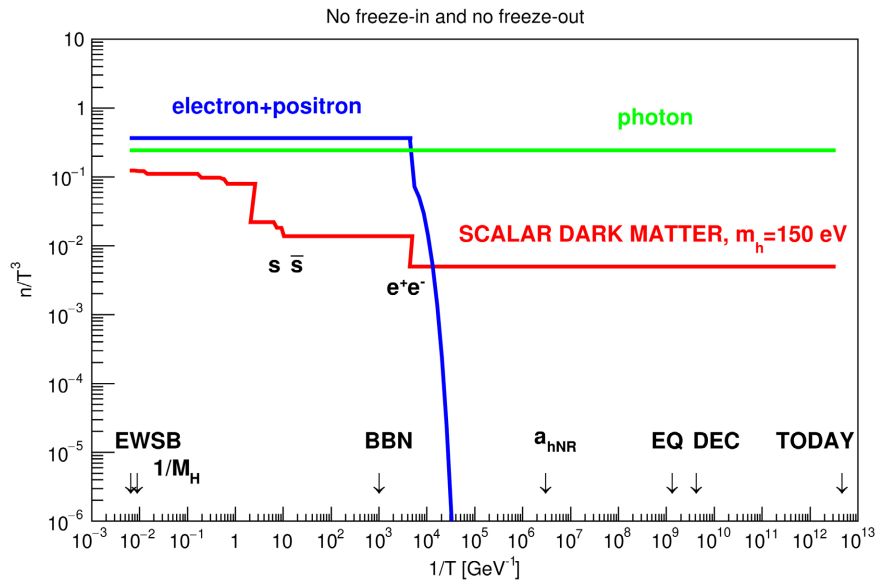


**Figure 5.** The no freeze-in and no freeze-out warm dark matter scenario is illustrated with an example.  $T$  is the photon temperature, and the  $n$ 's are particle number densities.

drops below  $M_H$ , (arguably) requires  $|\lambda_{hS}| > 7.4 \times 10^{-7}$  [25] (this limit depends on the physics before Electro-Weak Symmetry Breaking (EWSB)). The condition that the Higgs invisible decay width does not exceed the experimental bounds requires  $|\lambda_{hS}| < 0.03$  [25]. The cross-section per unit mass limit  $\sigma_{\text{DM-DM}}/m_h < 0.47 \text{ cm}^2/\text{g}$  [1] at  $a \approx 1$ , and Equation (13) of [25], imply  $\lambda_{hS} < 5.7 \times 10^{-5}$ , assuming  $\lambda_S$  is negligible. The measured cross-section per unit mass  $\sigma_{\text{DM-DM}}/m_h \approx (1.7 \pm 0.7) \times 10^{-4} \text{ cm}^2/\text{g}$  [26] at  $a \approx 1$ , and Equation (13) of [25], imply  $\lambda_{hS} = (7.8 \pm 0.9) \times 10^{-6}$  (this measurement needs confirmation). Note that there is a window of opportunity for  $\lambda_{hS}$ . The mass of the dark matter particle is  $m_h \equiv M_S = \sqrt{\lambda_{hS} v_h^2 / 2 + \bar{m}_S^2}$ , which requires fine tuning of  $\bar{m}_S^2$  [25].  $v_h \approx 246 \text{ GeV}$  is the Higgs boson vacuum expectation value. See **Figure 5**.

## 8. Conclusions

Our first measurement of dark matter velocity dispersion, based on ten spiral galaxy rotation curves measured by the THINGS collaboration, obtains  $v_{\text{rms}}(1) \equiv a_{\text{hNR}} c = 1.25 \pm 0.10(\text{stat}) \pm 0.75(\text{syst}) \text{ km/s}$ , predicts that this adiabatic invariant is of cosmological origin, and identifies that this measurement is consistent with the no freeze-in and no freeze-out warm dark matter scenario [3]. Every succeeding study reinforces this view: forty spiral galaxies of the SPARC sample [4], distributions of galaxy stellar masses [6], the formation of first galaxies and reionization [7], and the present study that includes the distributions of galaxy stellar masses and UV luminosities (10), reionization (11), and the velocity dispersion cut-off limit (12). All of these phenomena are consistent with the no freeze-in and no freeze-out warm dark matter scenario developed in [5], if dark matter particles have spin 0, and decouple early on from the standard model sector.

A summary of measurements is presented in **Table 3**. Note that we have *independently* and redundantly measured three observables of  $\Lambda$ WDM: the adiabatic invariant  $v_{\text{rms}}(1)$ , the delay of structure formation due to the free-streaming cut-off factor  $\tau^2(k)$ , *i.e.*  $k_{\text{fs}}(t_{\text{eq}})$ , and the velocity dispersion cut-off  $M_{\text{vd}}$ . And the three measured observables are consistent with each other. However, these measurements are in disagreement with several limits, of order keV, on the dark matter “thermal relic mass” that can be found in the literature. These limits on the “thermal relic mass” are really limits on  $k_{\text{fs}}(t_{\text{eq}})$  (whether or not we invoke the no freeze-in and no freeze-out scenario). The reason why the limits and measurements differ is that the limits neglect the non-linear regeneration of small scale structure (as studied in [5], and in section 3). The limits are corrected with even a tiny regenerated “tail” to  $\tau^2(k)$ , compared to tails obtained in simulations, see first two panels of **Figure 3**. Note that limits may rule out theories, but may not rule out measurements, if the measurements are correct. Therefore, may I suggest that the limits be revised, without neglecting the non-linear regenerated small scale structure (note its huge effect in [23]), and including the velocity dispersion cut-off mass (a phenomenon not included in the Press-Schechter

formalism). Let us mention that according to “The Review of Particle Physics” [1], limits on dark matter particle mass are  $m_h > 70$  eV for fermions, and  $m_h > 10^{-22}$  eV for bosons, and not several keV.

The measurements of  $v_{\text{hrms}}(1)$ , or equivalently  $k_{\text{fs}}(t_{\text{eq}})$ , determine the dark matter temperature-to-mass ratio, not separately the temperature or mass. The measured temperature-to-mass ratio happens to coincide with the no freeze-in and no freeze-out warm dark matter scenario prediction (as developed in [5]) if dark matter particles have spin 0, and decouple early on from the standard model sector. The cases of spin 1/2 and spin 1 are disfavored if nature has chosen the no freeze-in and no freeze-out scenario of [5], see Section 6.

In summary, a wealth of measurements redundantly confirm that dark matter is warm, and, barring a coincidence, obtain a detailed and precise no freeze-in and no freeze-out scenario of spin zero warm dark matter particles that decouple early on from the standard model sector.

### Conflicts of Interest

The author declares no conflicts of interest regarding the publication of this paper.

### References

- [1] Zyla, P.A., *et al.* (Particle Data Group) (2020) The Review of Particle Physics. *Progress of Theoretical and Experimental Physics*, **2020**, 083C01.
- [2] Boyanovsky, D., de Vega, H.J. and Sanchez, N.G. (2008) The Dark Matter Transfer Function: Free Streaming, Particle Statistics and Memory of Gravitational Clustering. *Physical Review D*, **78**, Article ID: 063546.
- [3] Hoeneisen, B. (2019) A Study of Dark Matter with Spiral Galaxy Rotation Curves. *International Journal of Astronomy and Astrophysics*, **9**, 71-96. <https://doi.org/10.4236/ijaa.2019.92007>
- [4] Hoeneisen, B. (2019) The Adiabatic Invariant of Dark Matter in Spiral Galaxies. *International Journal of Astronomy and Astrophysics*, **9**, 355-367.
- [5] Hoeneisen, B. (2022) Comments on Warm Dark Matter Measurements and Limits. *International Journal of Astronomy and Astrophysics*, **12**, 94-109. <https://doi.org/10.4236/ijaa.2022.121006>
- [6] Hoeneisen, B. (2020) Fermion or Boson Dark Matter? *International Journal of Astronomy and Astrophysics*, **10**, 203-223.
- [7] Hoeneisen, B. (2022) Warm Dark Matter and the Formation of First Galaxies. *Journal of Modern Physics*, **13**, 932-948.
- [8] Lapi, A., *et al.* (2017) Stellar Mass Function of Active and Quiescent Galaxies via the Continuity Equation. *The Astrophysical Journal*, **847**, Article No. 13. <https://doi.org/10.3847/1538-4357/aa88c9>
- [9] Song, M., Finkelstein, S.L., Ashby, M.L.N., *et al.* (2016) The Evolution of the Galaxy Stellar Mass Function at  $z = 4-8$ : A Steepening Low-Mass-End Slope with Increasing Redshift. *ApJ*, **825**, Article No. 5. <https://doi.org/10.3847/0004-637X/825/1/5>
- [10] Grazian, A., Fontana, A., Santini, P., *et al.* (2015) The Galaxy Stellar Mass Function at  $3.5 \leq z \leq 7.5$  in the CANDELS/UDS, GOODS-South, and HUDF Fields. *Astron-*

- omy and Astrophysics*, **575**, A96.
- [11] Davidzon, I., Ilbert, O., Laigle, C., *et al.* (2017) The COSMOS2015 Galaxy Stellar Mass Function: 13 Billion Years of Stellar Mass Assembly in 10 Snapshots. *Astronomy and Astrophysics*, **605**, A70. <https://doi.org/10.1051/0004-6361/201730419>
- [12] Lapi, A. and Danese, L. (2015) Cold or Warm? Constraining Dark Matter with Primeval Galaxies and Cosmic Reionization after Planck. *Journal of Cosmology and Astroparticle Physics*, **9**, Article No. 3. <https://doi.org/10.1088/1475-7516/2015/09/003>
- [13] Bouwens, R.J., *et al.* (2015) UV Luminosity Functions at Redshifts  $z \approx 4$  to  $z \approx 10$ : 10000 Galaxies from HST Legacy Fields. *The Astrophysical Journal*, **803**, Article No. 34. <https://doi.org/10.1088/0004-637X/803/1/34>
- [14] Bouwens, R.J., *et al.* (2021) New Determinations of the UV Luminosity Functions from  $z \approx 9$  to  $z \approx 4$  Show a Remarkable Consistency with Halo Growth and a Constant Star Formation Efficiency. *The Astronomical Journal*, **162**, Article No. 47. <https://doi.org/10.3847/1538-3881/abf83e>
- [15] McLeod, D.J., *et al.* (2015) New Redshift  $z \approx 9$  Galaxies in the Hubble Frontier Fields: Implications for Early Evolution of the UV Luminosity Density. *MNRAS*, **450**, 3032-3044.
- [16] Bouwens, R.J., Illingworth, G.D. and Oesch, P.A. (2014) UV-Continuum Slopes of 4000  $z \approx 4$ -8 Galaxies from the HUDF/XDF, HUDF09, ERS, CANDELS-South, and CANDELS-North Fields. *The Astrophysical Journal*, **793**, Article No. 115. <https://doi.org/10.1088/0004-637X/793/2/115>
- [17] Press, W.H. and Schechter, P. (1974) Formation of Galaxies and Clusters of Galaxies by Self-Similar Gravitational Condensation. *The Astrophysical Journal*, **187**, 425-438. <https://doi.org/10.1086/152650>
- [18] Sheth, R.K. and Tormen, G. (1999) Large-Scale Bias and the Peak Background Split. *Monthly Notices of the Royal Astronomical Society*, **308**, 119-126. <https://doi.org/10.1046/j.1365-8711.1999.02692.x>
- [19] Sheth, R.K., Mo, H.J. and Tormen, G. (2001) Ellipsoidal Collapse and an Improved Model for the Number and Spatial Distribution of Dark Matter Haloes. *Monthly Notices of the Royal Astronomical Society*, **323**, 1-12. <https://doi.org/10.1046/j.1365-8711.2001.04006.x>
- [20] Weinberg, S. (2008) *Cosmology*. Oxford University Press, Oxford.
- [21] Hoeneisen, B. (2021) A Study of Three Galaxy Types, Galaxy Formation, and Warm Dark Matter. *International Journal of Astronomy and Astrophysics*, **11**, 489-508. <https://doi.org/10.4236/ijaa.2021.114026>
- [22] Madau, P., Pozzetti, L. and Dickinson, M. (1997) The Star Formation History of Field Galaxies. *The Astrophysical Journal*, **498**, Article No. 106. <https://doi.org/10.1086/305523>
- [23] White, M. and Croft, A.A.C. (2018) Suppressing Linear Power on Dwarf Galaxy Halo Scales. *The Astrophysical Journal*, **539**, 497-504. <https://doi.org/10.1086/309273>
- [24] Mason, C.A., Trenti, M. and Treu, T. (2015) The Galaxy UV Luminosity Function Before the Epoch of Reionization. *The Astrophysical Journal*, **813**, Article No. 21. <https://doi.org/10.1088/0004-637X/813/1/21>
- [25] Hoeneisen, B. (2021) Adding Dark Matter to the Standard Model. *International Journal of Astronomy and Astrophysics*, **11**, 59-72. <https://doi.org/10.4236/ijaa.2021.111004>

- [26] Massey, R., *et al.* (2015) The Behaviour of Dark Matter Associated with 4 Bright Cluster Galaxies in the 10kpc Core of Abell 3827. *Monthly Notices of the Royal Astronomical Society*, **449**, 3393-3406. <https://doi.org/10.1093/mnras/stv467>